Long Distance Ranging Performance of Gen3 LiDAR Imaging System based on 1x16 SiPM Array

Salvatore Gnecchi, Colin Barry, Stephen Bellis, Steve Buckley, Carl Jackson
SensL Division, ON Semiconductor, 6800, Cork Ariport Business Park, Cork, Ireland

***Abstract*—An imaging LiDAR demonstration system is presented. Outdoors long distance measurements are taken to validate the modelled performance of a silicon photomultiplier (SiPM) based sensor for LiDAR. A complete link budget is provided for the coaxial system used for the testing. A 1×16 SiPM array is presented and modelled. The demonstration system achieves a resolution of $0.1^\circ \times 0.3^\circ$ over a total $80^\circ \times 5^\circ$ giving a 800×16 depth map. Outdoors measurements show ranging capabilities in full sunlight outdoor environment with maximum distances of $40\mathrm{m}$ with a target albedo of 12% and beyond $80\mathrm{m}$ for 84% albedo all in $130\mathrm{klx}$ sunlight. The validation of the presented model paves the road to commercial LiDAR systems achieving 200+ m ranging.**

***Index Terms*—LiDAR, silicon photomultiplier, SiPM, time-of-flight.**

I. Introduction

The automotive industry has focused its attention on LiDAR for Assisted Driving Automotive Systems (ADAS) and the ultimate Autonomous Driving (AD) systems [1]–[3]. The main challenge for such sensors is determined by harsh ambient light conditions and low-reflective targets which impact the maximum distance ranging performance at eye-safe low laser powers [4]. Two main methods are available to illuminate a large filed-of-view (FoV) scene: a flash mode, where all the scene is illuminated at the same time; and a beam steered mode, where only a section of the scene (point, line or cluster) is illuminated sequentially in a full scan of the scene. The latter allows for a better power usage achieving a higher power density over the large scene thus improving the long ranging performance. Research and commercial works show different implementations of systems where the laser light is scanned over the scene and the receiver angle-of-view (AoV) follows the illuminated scene in a co-axial architecture achieving medium to long distance ranging performance in a variety of target and ambient conditions [5]–[7].

We show through a demonstration system the ranging abilities of a silicon photomultiplier based scanning LiDAR, Fig.1. A previously introduced model is coupled here with a complete link budget and demonstrated on hardware [8]. The validation through real-life data of the proposed analytical model offers a strong tool to pave the road to long distance range LiDAR systems by understanding the system requirements and challenges.

Section II introduces the demonstration system in all its components. The link budget and subsequent ranging model is detailed in Section III. The validation of the model is presented in Section IV. Outlook and conclusions are provided in the final Section V.

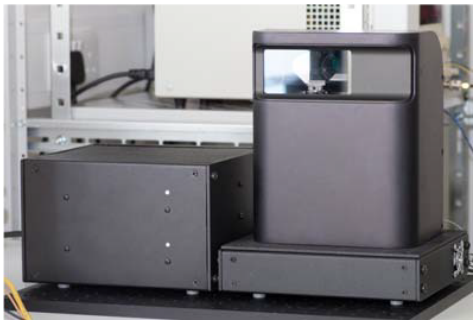

(a)

(b)

Fig. 1. SensL Gen3 - Demonstration system based on SiPM array. System photograph (a) and detector board (b)

II. The Gen3 Demonstration System

The SensL Gen3 LiDAR imaging system is based on a coaxial architecture, as shown in Fig.2. The emitter part of the system generates a laser line through 16 $905\mathrm{nm}$ laser diodes with $400\mathrm{W}$ peak power over a $1\mathrm{ns}$ FWHM pulse width [9]. Collimating lenses are used to set the shape of the beam. Its horizontal divergence sets the angular resolution of the

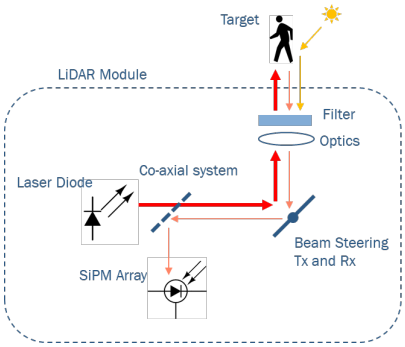

Fig. 2. A coaxial LiDAR system

system and its vertical divergence the total angle of view in the same direction. These two are respectively $0.1°$ and $5°$. On the transmitter path, two main components are present: a beam splitter and a galvo. The former element is necessary due to the coaxial architecture of the system: it allows for the transmitted and return light to share the same optical path, as shown in Fig.2. This way, the electro-mechanical steering element, the galvo, is able to not only scan the emitted light onto the scene but also to scan the AoV of the detector. The divergence of the emitter beam and the AoV of the sensor have been matched for an optimal signal-to-noise ratio.

On the receiver path, the light directed from the mirror of the galvo onto the beam splitter is then collected by a lens, filtered through a bandpass around the chosen wavelength and then directed onto the receiving SiPM detector. Each of the 16 elements of the array is connected through a read out channel: a voltage amplifier, a fast comparator with individual programmable threshold and a FPGA time to digital converter (TDC). The output of the TDC is then fed into the memory of the FPGA which stores a histogram from which a time-of-flight (ToF) stamp is extracted through peak detection. The collected ToF stamps are then read out by a software that converts them into distance measurements and plots them into a depth map. Histograms can alternatively streamed out for statistical analysis. This is here done to validate the analytical model.

In the next section, the link budget is discussed and the model presented.

III. Link Budget and Ranging Model

A summary of the main system parameters is described in Table I (updated from previous work only in the photo detection efficiency (PDE) of the SiPM [8]). In this section we consider the optical losses in both emitter and receiver path due to non-ideal components. Starting from the transmitter path, the light goes through a series of elements as described in Section II. The main contribution to the optical losses in this path is given by the collimating lenses which have a transmission efficiency of about 87%. All the rest of the components have efficiency values between 98-99.5%. Together with the efficiency of the laser diode (estimated as 90%), the total transmitter efficiency is calculated as:

$$\varepsilon_{\mathtt{TX}} = 68.7\% \tag{1}$$

Eq. (1) shows how more than 30% of the laser power is effectively lost before leaving the unit, highlighting room of improvement for future non-coaxial systems. In the return path, the two main contributions are identified: the beam splitter and the bandpass filter. Only 45% of the light is redirected towards the SiPM array by the beam splitter. Considering all the components (mirror, collecting lenses, filter, etc.) the calculated efficiency of the receiver path is:

$$\varepsilon_{\mathtt{RX}} = 37\% \tag{2}$$

Combining (1) and (2), only 25.42% of the emitted laser power is sensed by the system purely due to non-ideal components.

TABLE I
SensL Gen3 System Parameters*

Parameter	Value
Array size	1×16
SiPM pixel length x	$171\,\mu\mathrm{m}$
SiPM pixel height y_1	$491\,\mu\mathrm{m}$
Pixel spacing y_2	$59\,\mu\mathrm{m}$
Total array length y_3	$8.741\,\mathrm{mm}$
SPAD cells per pixel N_{cells}	133
PDE @ $905\,\mathrm{nm}$	$3.5\,\%$
SPAD cell dead time τ_{dead}	23ns
SiPM pixel gain G	10^6
SiPM rise time τ_{rise}	$100\,\mathrm{ps}$
Laser divergence	$0.1° \times 5°$
Laser peak power P_{laser}	$400\,\mathrm{W}$
Laser pulse width τ_{pulse}	$1\,\mathrm{ns}$
Laser pulse repetition rate PRR	$500\,\mathrm{kHz}$
Frames per second	$30\,\mathrm{fps}$
Optical aperture D_{lens}	$22\,\mathrm{mm}$
Scanning angle of view	$80° \times 5°$
Static angle of view $AoV_x \times AoV_y$	$< 0.1° \times 5°$
Angular resolution	$0.1° \times 0.312°$
Optical bandpass $\lambda \pm \Delta\lambda$	$(905 \pm 25)\,\mathrm{nm}$

*Higher PDE SiPM are now commercially availably through ON Semiconductor / SensL Division

These two quantities $\varepsilon_{\mathtt{TX}}$ and $\varepsilon_{\mathtt{RX}}$ need to be used in the calculation the amount of signal and noise incident on the SiPM sensors. Following already published equations, we estimate the signal and noise onto the sensor as the average number of cells in each SiPM pixel firing due to respectively return laser echo and uncorrelated ambient noise [8]. We re-write the two equations explicitly highlighting the new parameters introduced by the detailed link budget. The two equations become:

$$N_{amb} = N_{cells} \cdot \left(1 - e^{-\varepsilon_{\mathtt{RX}} \cdot \Phi_{amb} \cdot PDE \cdot \tau_{dead}/N_{cells}}\right) \tag{3}$$

$$N_{laser}(d) = (N_{cells} - N_{amb}) \times \left(1 - e^{-\varepsilon_{\mathtt{RX}} \cdot \varepsilon_{\mathtt{TX}} \cdot \Phi_{return} \cdot PDE \cdot \tau_{pulse}/N_{cells}}\right) \tag{4}$$

The authors redirect the readers to the previous publication for the definition of each of the parameters in both (3) and (4). The rest of the analysis remains unaltered and the probability of successful ranging can be calculated for any ambient light and target albedo values. We recall here the estimated probability of ranging in histogram mode with $\mathcal{N}_{shots}$ multi-shots as:

$$p_{multishot}(d) = \sum_{k=\mathcal{N}_{uns}+1}^{\mathcal{N}_{shots}} \binom{\mathcal{N}_{shots}}{k} \times p_{success}(d)^k \times \times \left[1 - p_{success}(d)\right]^{\mathcal{N}_{shots}-k} \tag{5}$$

Eq. (5) will be used to plot the estimated success rate of ranging against the target distance in the next Section IV.

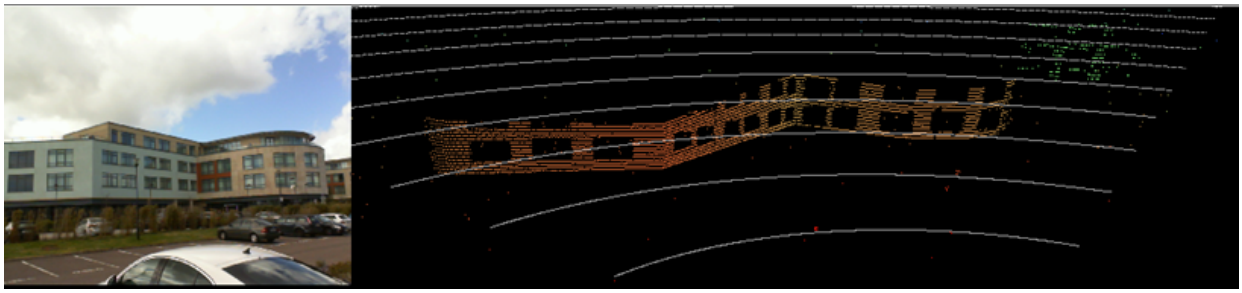

Fig. 3. Depth map of outdoors scenario in full imaging mode beside a regular camera image showing the scenario

IV. Test Procedure and Results

The LiDAR system here presented in Section II has been tested outdoors demonstrating ambient light robustness, see Fig. 3. To validate the modelling developed and applied to this system, the demonstrator has been utilised with two targets each with a calibrated albedo at $905\mathrm{nm}$ wavelength. An 84% reflective material has been chosen as a bright object and a 12% as a dark one. The materials have been put on a target whose size has been chosen so that the entire target can be imaged on one or more pixels throughout all the measuring distances. This allows us to assume that none of the laser power per pixel is lost due to a small target and that the background (of unknown reflectivity) does not contribute to the noise level. To validate the model, the unit has been utilised in a non-scanning mode where the sensor points at a fixed direction without any movement of the galvo. This enables the recording and collection of entire histograms from each of the channels.

The aim of these tests is to determine, after the acquisition of each histogram, the success rate of the ranging experiment at a given distance / target albedo. To do so, the two targets are alternatively positioned from short to longer distance away from the LiDAR unit. At each distance step, histograms are collected. To enable a statistical relevance of the data, a thousand histograms are collected per each step. Each of the histograms is off-line processed to extract the ToF / distance. Each histogram has a binary value of 1 or 0 assigned respectively if the extracted distance matches or differs from the actual value. By averaging the 1/0s over the full thousand trials, a success rate is calculated per each ranging distance. This is directly compared to the computed probability of ranging expressed by (5). Moreover, to assign an error to the extracted probability, the set of 1000 histograms has been divided in 40 subsets of 25 histograms each. Minimum and maximum values have been extracted from these 40 success rate values. These are used to create error bar plots to help the visual comparison between real data and calculated probability.

All the tests took place in an outdoor scene on a sunny day with variable ambient light level est imated with a lux-meter within a range of 10 to 130 klx. The variable forecast impacting the noise level during the acquisition of the data had to be taken into account. When plotting the acquired data, a colour coded mark has been utilised to indicate the average ambient light level during the acquisition of the histograms used to extract each average value. The model has been computed and plotted using a low and a high value margin between which the data are expected to be contained.

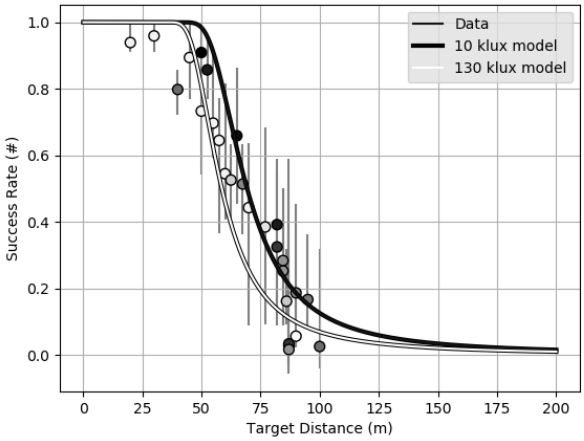

(a)

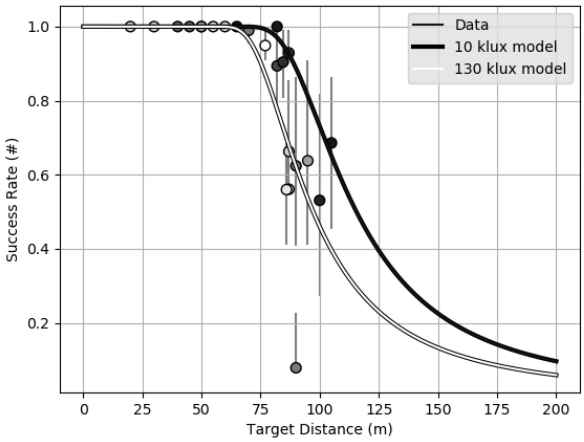

(b)

Fig. 4. Ranging performance of a dark target with (a) 20 laser shots per measurements and (b) 100 laser shots

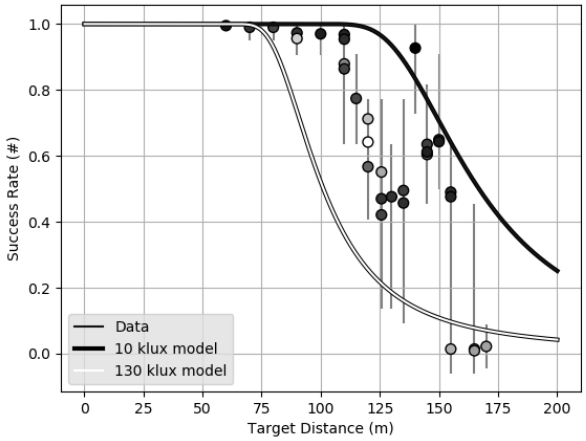

(a)

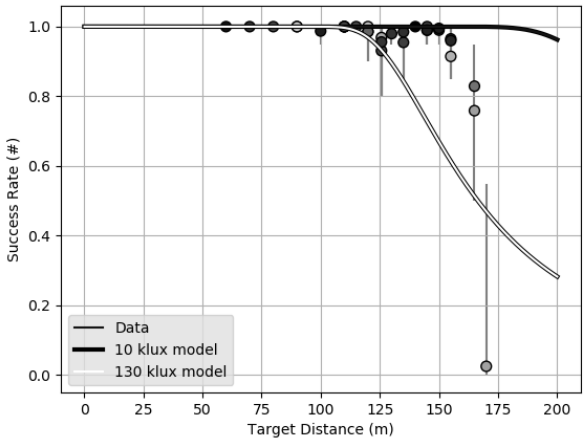

(b)

Fig. 5. Ranging performance of a bright target with (a) 20 laser shots per measurements and (b) 100 laser shots

Fig. 4 shows the results of the ranging tests for the dark target. Two options were simulated. Fig. 4(a) shows both data and model results using 20 multi-shot per measurement (per histogram). This scenario has been chosen to represent the operation of the demonstration system at 30 frames per second with a laser repetition rate of $500\mathrm{kHz}$ (as specified in Table I). The plot shows successful ranging beyond $40\mathrm{m}$ with a detection probability higher than 99%.

Fig. 4(b) shows instead the result of the same test but using 100 multi-shots per histogram. This has been done to validate the model in more than one scenario. Although the ambient light conditions caused a serious variation on the collected set of data, including a few off-the-trend points, the model is here verified to well describe the ranging experiment.

For completeness, we provide results for ranging experiments with a bright target, see Fig. 5. As expected, the performance is improved due to a higher signal to noise ratio. A longer ranging performance of beyond $80\mathrm{m}$ is demonstrated in a 30 frame per second operation (20 shots) as shown in Fig.5(a).

V. Outlook and Conclusions

We have successfully presented the validation of a ranging model for SiPM based sensor with a horizontal scanning LiDAR system based on electromechanical coaxial scan. A $40\mathrm{m}$ ranging performance has been demonstrated in harsh ambient light conditions and low target reflectivity with eye safe laser power.

The validated model represents a tool to determine the impact of each of the parameters of a LiDAR system in terms of ranging ability in all given scenarios. The outlook of this work is to use the validated model to design the future generation of LiDAR systems achieving longer ranging distances $(200 + \mathrm{m})$ in all ambient light conditions as the automotive industry is demanding.

References

[1] R. Thakur, "Scanning LIDAR in Advanced Driver Assistance Systems and Beyond: Building a road map for next-generation LIDAR technology," *IEEE Consumer Electronics Magazine*, vol. 5, no. 3, pp. 48–54, 2016.

[2] A. Ziebinski, R. Cupek, H. Erdogan, and S. Waechter, "A survey of ADAS technologies for the future perspective of sensor fusion," *Lecture Notes in Computer Science (including subseries Lecture Notes in Artificial Intelligence and Lecture Notes in Bioinformatics)*, 2016.

[3] E. Ackerman, "Lidar that will make self-driving cars affordable [News]," *IEEE Spectrum*, vol. 53, no. 10, pp. 14–14, 2016.

[4] M. Kutila, P. Pyykönen, W. Ritter, O. Sawade, and B. Schäufele, "Automotive LIDAR sensor development scenarios for harsh weather conditions," *IEEE Conference on Intelligent Transportation Systems, Proceedings, ITSC*, pp. 265–270, 2016.

[5] A. McCarthy, R. J. Collins, N. J. Krichel, V. Fernández, A. M. Wallace, and G. S. Buller, "Long-range time-of-flight scanning sensor based on high-speed time-correlated single-photon counting," *Applied Optics*, vol. 48, no. 32, p. 6241, nov 2009. [Online]. Available: https://www.osapublishing.org/abstract.cfm?URI=ao-48-32-6241

[6] C. Niclass, M. Soga, H. Matsubara, S. Kato, and M. Kagami, "A 100-m range 10-Frame/s 340, 96-pixel time-of-flight depth sensor in 0.18-μm CMOS," *IEEE Journal of Solid-State Circuits*, vol. 48, no. 2, pp. 559–572, 2013.

[7] Velodyne LiDAR, "Hdl-64E," 2016.

[8] S. Gnecchi and C. Jackson, "A 1 16 SiPM Array for Automotive 3D Imaging LiDAR Systems," *International Image Sensor Society*, pp. 133–136, 2017.

[9] "OSRAM: www.osram.com."